A High-Field High-Frequency Permeance Meter For Thin-Film Materials

H. Mukadam
C. R. Sullivan
S. Prabhakaran

Found in *IEEE Power Electronics Specialists Conference,* June 2008, pp. 4044–4050.

A High-Field High-Frequency Permeance Meter for Thin-Film Materials

Hozefa Mukadam
hozefa.mukadam@dartmouth.edu

Charles R. Sullivan
chrs@dartmouth.edu

Thayer School of Engineering at Dartmouth
8000 Cummings Hall, Hanover, NH 03755 USA
http://power.thayer.dartmouth.edu

Satish Prabhakaran
prabhaka@ge.com
GE Global Research
1 Research Circle Building
Niskayuna, NY 12309 USA

***Abstract*—Inductors using thin-film magnetic cores are attractive for high-frequency power converters. For developing accurate loss models for these inductors complex permeability measurements of the thin-film core materials have to be made at high magnetic fields and high frequencies. We describe a high-field high-frequency permeance meter capable of measuring complex permeability of thin-film materials in the 50 MHz frequency range with applied fields up to about 100 Oe.**

I. Introduction

Very-high-frequency (30-300 MHz) dc/dc converters using air-core inductors have been reported [1]–[4]. The performance of these converters can be improved by using high-frequency high-power inductors designed with thin-film magnetic cores [5]–[7]. The thin film in these inductors is subjected to magnetic fields in the 100 Oe range and in order to accurately develop loss models for these inductors it is important to measure the losses in the thin-film magnetic material at high fields and high frequencies.

Presently available permeance meters such as those described in [8]–[13] can measure the complex permeability of thin-film materials up to the GHz range. However, these permeance meters are limited to measurements at excitation fields in the mOe range [8], [9]. We describe a high-field high-frequency permeance meter capable of measuring complex permeability in the 50 MHz frequency range with applied fields up to about 100 Oe.

II. Principle

The permeance meter is based on the transformer principle in which an ac field is developed in a drive coil and the signal is detected in a pick-up coil [12], [13]. The drive field is produced in an inductor cavity which is a part of an LC resonator drive circuit. A pick-up coil is placed in the cavity (see Fig. 1) and the voltage induced in the coil with no sample in the coil is measured. Then a magnetic sample is placed through the pick-up coil and the induced voltage is measured again. The ratio of the two voltages is used to calculate the relative permeability of the magnetic material.

III. Design and Construction

The measurement system comprises a resonant field generator to apply a high field to a sample, pick-up coils in which signals are induced, and instrumentation to measure these signals which are then used to calculate the permeability of the magnetic material.

A. Resonant Field Generator

The field generation system consists of two matched single-turn cavities machined out of a copper block and connected in series. Provisions were made during machining to solder surface-mount capacitors across the ends of the cavities. With the capacitors connected as shown in Fig. 1, the structure forms a parallel LC circuit that can resonate at the frequency of interest. An amplifier drives this resonant circuit through a 700 nH tuning coil to match the high impedance of the resonant circuit to the 50 Ω output of the amplifier. Using an LC circuit minimizes the current drawn from the amplifier to achieve a given field in the cavities thus minimizing the power losses in the cables and connectors leading to the LC circuit and making it possible to achieve a high field without requiring an extremely powerful amplifier.

The purpose of the dual-cavity design is to allow the use of a second pick-up coil placed in the second cavity to provide a reference signal to calibrate the phase of the measurement in the first cavity. Moreover, the second cavity allows accurate measurement of the current (and hence applied field) in the resonant cavities without affecting the permeability measurement in the adjacent cavity.

The cavities were designed to each provide a peak field of 100 Oe at a peak current of nearly 150 A in resonance. They were rounded at the corners (not shown in Fig. 1) to avoid current crowding at the edges. As determined by finite element analysis (FEA), the two cavities exhibit a total

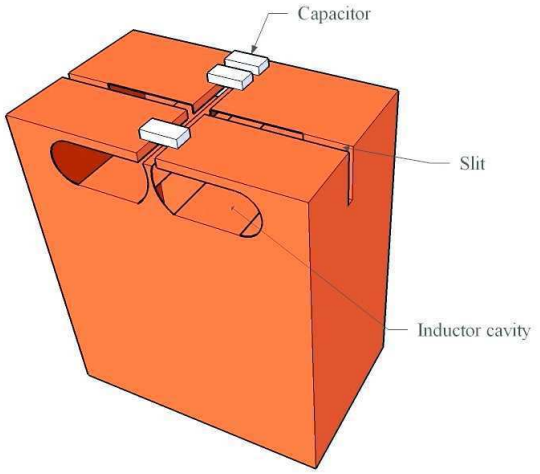

Fig. 1. Schematic of the resonator block showing inductor cavities, capacitors and slits.

978-1-4244-1668-4/08/$25.00 ©2008 IEEE

series inductance of $L_{cav} = 6.6$ nH. Three surface-mount capacitors, each 430 pF, were soldered across the ends of the cavities so that total capacitance, $C_{cav} = 1.29$ nF. The resonance frequency of the circuit was expected to be nearly 54 MHz. The total ac resistance of the two resonator cavities was estimated by FEA to be $R_{cav} = 5$ mΩ.

B. Pick-Up Coils

A trace of copper on a polyimide substrate implements the single-turn pick-up coil. The polyimide substrate is placed in the cavities through slits cut on the two sides of the copper block such that the area vector of the pick-up coil is parallel to the magnetic field in the cavity. The pick-up coil consists of a single loop of 18 μm $\times$ 50 μm copper on a 650-μm-thick polyimide substrate. The substrate has a 5 mm $\times$ 2 mm window inside the loop as shown in Fig. 2 for inserting the sample. The magnetic samples we were interested in characterizing are described in detail in Section V-A. The samples exhibit significant magnetic anisotropy in the plane of the film [14], [15]. The magnetization of the sample aligns in one axis, the *easy axis*, in the absence of an applied field. Magnetization in the plane, but perpendicular to the easy axis, along the *hard axis* results in a hysteresis loop which has nearly zero area, and thus this direction is preferred for low-loss operation. The sample is positioned in the cavity such that the applied field is parallel to the hard axis of the sample. The signal induced in the pick-up coil is due to the flux along this axis. The signal from the pick-up coil is attenuated and matched to a 50-Ω transmission line. A voltage divider for this purpose is implemented on the same polyimide substrate. The measurements are taken on an Agilent 8753E network analyzer.

C. Common-Mode Chokes

Prior to being measured on the network analyzer, the signal from the attenuation network is passed through a common-mode choke connected between the attenuation network and the measurement channel of the network analyzer. The function of the common-mode choke is to reduce the effect of common-mode voltages induced in the pick-up coil as a result of second-order coupling effects between the pick-up coil and resonator (see Section V-B). The magnetic core for the chokes was made using nickel-zinc ferrite rods [16]. Four rods, each cut at a 45° angle, were mated together to form a square core. Four such cores were stacked to form a composite core and six turns of semi-rigid coaxial cable were then wound on it to form a common-mode choke. The design value of the magnetizing impedance was 4.7 kΩ at 55 MHz. The impedance as measured by an Agilent 4294A impedance analyzer was found to be around 2 kΩ and it was capacitive in the 50 MHz region. This is attributed to the interwinding capacitance. The coaxial cables were passed through teflon tubing to increase the separation between the windings and hence reduce the interwinding capacitance.

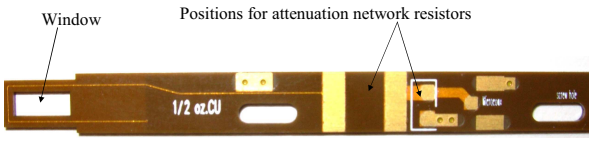

Fig. 2. Photograph of the pick-up coil and the attenuation network designed on a polyimide substrate. Also shown is the window on the substrate for inserting a thin-film sample.

IV. Theory of Operation

For a single-turn pick-up coil loop placed in a magnetic field of intensity H, the complex phasor voltages induced with and without the sample are:

$$V_{without} = j2\pi f H \mu_0 A_{pickup} \tag{1}$$

$$V_{with} = j2\pi f \mu_0 H \Big[\mu^* A_{sample} + (A_{pickup} - A_{sample})\Big] \tag{2}$$

where A_{pickup} is the area enclosed by the pick-up coil loop inside the cavity and A_{sample} is the cross sectional area of a sample placed through the loop. μ_0 is the permeability of free space, f is the frequency, and μ^* is the complex permeability of the magnetic sample which can be written from (1) and (2)

$$\mu^* = \frac{A_{pickup}}{A_{sample}} \left(\frac{V_{with-sample}}{V_{without-sample}} - 1 \right) + 1 \tag{3}$$

A_{pickup} and A_{sample} are known dimensions; phasors $V_{with-sample}$ and $V_{without-sample}$ are measured precisely using a network analyzer to yield the complex permeability of the magnetic sample.

V. Errors— Analysis and Mitigation

In this section we discuss different sources of error in μ^* measurement of thin-film magnetic material. The thin-film material that we have tested consists of cobalt nano particles dispersed in a zirconium oxide matrix. Work has been reported in [15], [17]–[20] regarding the fabrication and properties of Co-Zr-O thin-films. Our test samples were fabricated by RF sputtering on a 50 μm thick polyimide substrate in an Ar + O_2 environment using Co-Zr alloy target. A Halbach [21] array provided a uniform magnetic field of 400 Oe in order to introduce a uniform uniaxial anisotropy in the magnetic film during deposition. 6 μm thick magnetic material was deposited on each side of the substrate. The samples were 2 mm wide. Hence the cross sectional area of the magnetic material is 2 mm $\times$ 12 μm.

In a low-loss material, μ'' is expected to be small and hence the phase difference θ between the measured voltage phasors with and without the sample is small so that $\sin(\theta) \approx \theta$ and the imaginary component of (3) can be written as

$$\mu'' = \frac{A_{pickup}}{A_{sample}} \left| \frac{V_{with-sample}}{V_{without-sample}} \right| \theta \tag{4}$$

The ratio of pick-up coil to sample area for our coil and sample geometries is approximately 1190. A nominal ratio

of voltages induced in the pick-up coil with and without the sample, measured with the single-loop pick-up coil as described in Section III-B and, at the resonant frequency of the LC resonator, is 1.04. With this data, (4) gives

$$\mu^{''} = 1235 \cdot \theta \tag{5}$$

From (5) one can see that any small error in the phase difference measurement will result in a huge error in the imaginary permeability measurement. Many such errors are minimized by measuring a ratio of the signals picked up from the two cavities. However, the quantity which we are trying to measure can be easily suppressed by any systematic error or noise in the measurements. In order to make useful measurements, we studied the errors present in the system and then devised ways to eliminate or reduce them.

A. Resonant Frequency Shift and Circulating Current Analysis

The resonant frequency of the system represented in Fig. 3 is defined as the frequency at which the magnitude of current circulating in the resonator cavities is maximized. When no sample is placed in the cavity, we denote the resonant frequency by f_{wo} and the circulating current by I_{wo}. The inductance of the resonator cavities increase from L_{cav} to L_{cav-w} when a sample is placed in one of the cavities and hence the resonant frequency of the system is different than it was without a sample. We devised methods to keep the system at resonance with a sample in place and hence maintain the current circulating in the cavities unchanged.

One method to maintain the system at resonance when a sample is in place is to operate the system at its new resonant frequency. We denote this frequency by f_w and the circulating current by I_{w,f_w}.

Another approach is to use a trimmer capacitor in parallel with LC resonator capacitors. In order to calculate the value of the trimmer capacitor required to maintain the system at resonance when a sample is in place, we take a closer look at the circuit in Fig. 3. The capacitance represented as C_{cav} in Fig. 3 can be considered as a parallel combination of two capacitances. First among this is a capacitance which, together with inductance L_{cav}, forms the parallel LC resonator. The second one, which is less than 1% of C_{cav}, together with the tuning inductor L_{tun}, matches the high impedance of the parallel LC circuit to a 50-Ω drive. An approximate value of the trimmer capacitance C_{trim} required can be calculated by noting that C_{cav} consists almost entirely of the resonator capacitance. C_{trim}, the capacitance which maintains the resonant frequency at f_{wo}, and is the difference of C_{cav} and C_{cav-w}, can then be given by

$$C_{trim} = C_{cav}\left[1 - \left(\frac{f_w}{f_{wo}}\right)\right]^2 \tag{6}$$

The circulating current, when such a trimmer capacitor is employed, is denoted by I_{trim}. A trimmer capacitor having C_{trim} in its adjustable range was used and its value was adjusted until the circulating current in the cavities was maximized.

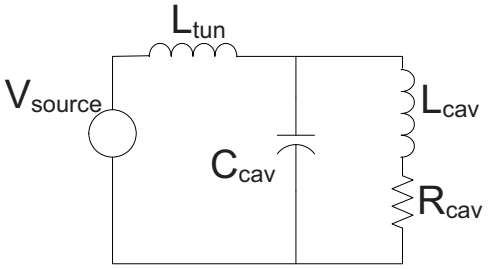

Fig. 3. Schematic showing the LC resonator and the tuning coil.

TABLE I
RESONATOR CIRCUIT QUANTITIES

Quantity	Value
L_{tun}	700 nH
L_{cav}	6.6 nH
C_{cav}	1.298 nF
R_{cav}	5 mΩ
L_{cav-w}	6.611 nH
C_{trim}	2.4 pF

L_{cav-w} and C_{trim} are specific to the thin-film sample described in Section V

Table I lists the quantities needed to evaluate the different circulating currents. Table II lists the currents I_{wo}, $I_{w,f_{wo}}$ and I_{trim} evaluated at $f_{wo} = 54.63$ MHz and I_{w,f_w} evaluated at $f_w = 54.58$ MHz. V_{source} has been taken as 8 V. From Table II we see that the circulating current

TABLE II
CIRCULATING CURRENT VALUES

Quantity	Magnitude	Phase (w.r.t. V_{source})
I_{wo}	15.07 A	2.01°
$I_{w,f_{wo}}$	12.34 A	324.98°
I_{w,f_w}	14.98 A	324.98°
I_{trim}	14.97 A	7.636°

changes its magnitude by 18% when no step is taken towards maintaining the system in resonance when a sample is placed in the cavity. The change in circulating current, when the operating frequency of the system is changed to its new resonant frequency, is less than 1%. The dual-frequency operation maintains the circulating current almost unchanged but introduces a phase error resulting from mismatches in the attenuation network. This phase error, as found out by measuring the phase difference between the reference and test pick-up coils across frequency, was 0.01° which would result in an error in $\mu^{''}$ measurement of about 0.2. We decided not to use this method for maintaining resonance.

On the other hand, using a trimmer capacitor ensures the circulating current in the cavities is approximately unchanged when a sample is placed in the cavity, without introducing additional phase errors.

TABLE III
PICK-UP COIL CIRCUIT QUANTITIES

Parameter	Explanation	Value
V_{ind}	Voltage induced in the pick-up coil	See (7) and (8)
$V_{leak-small}$	Voltage induced in the small leakage voltage loop	See (9)
$V_{leak-big}$	Voltage induced in the big leakage voltage loop	See (10)
L_{self}	Self inductance of the pick-up coil	25 nH
R_1	Attenuation resistor	2.49 kΩ
R_2	Impedance matching resistor	50 Ω
$R_2^{'}$	Network analyzer resistor	50 Ω
C_{P1}, C_{P2}	Parasitic capacitance between the pick-up coil and resonator block	0.5 pF each
$R_{CM,pkp}$, $C_{CM,pkp}$	Impedance of the common-mode choke connected to the pick-up coil	490 Ω, 1.3 pF
$R_{CM,resonator}$, $C_{CM,resonator}$	Impedance of the common-mode choke connected to the resonator	390 Ω, 6.3 pF
C_{leak}	Capacitance between resonator block and main enclosure	12 pF
V_{meas}	Voltage measured by the network analyzer	

B. Pick-Up Coil Circuit

As explained in Section III-B, the pick-up coil is a single trace of copper on a polyimide substrate and it is placed in the resonator cavity through the slit on the resonator block. In order to accurately model the behavior of the pick-up coil, in addition to the magnetic coupling between the pick-up coil and the resonator block in the cavity, we have to consider the secondary coupling effects between the pick-up coil and the resonator block as well. In this section we develop an equivalent circuit model of the pick-up coil placed in the resonator cavity.

Fig. 4 is a schematic of the pick-up coil placed in the resonator cavity. The flux linkage loop between the resonator cavity and the pick-up coil is shown. Also shown are the two ground loops resulting in induced voltages due to leakage flux in the main enclosure. The two coupling capacitances represent the capacitive coupling between the copper traces on polyimide and the resonator block. The attenuation network and the common mode choke are shown as well.

Fig. 5 is an equivalent circuit obtained from the schematic in Fig. 4 and Table III lists all the quantities represented in Fig. 5. The coupling capacitance between the pick-up coil and the resonator block as measured by the impedance analyzer was around 1 pF. We have assumed equal values for C_{P1} and C_{P2} and each of them is taken as 0.5 pF. CM, pkp and $CM, resonator$ (not shown in Fig. 4) represent the common-mode chokes connected to the pick-up coil and resonator block, respectively.

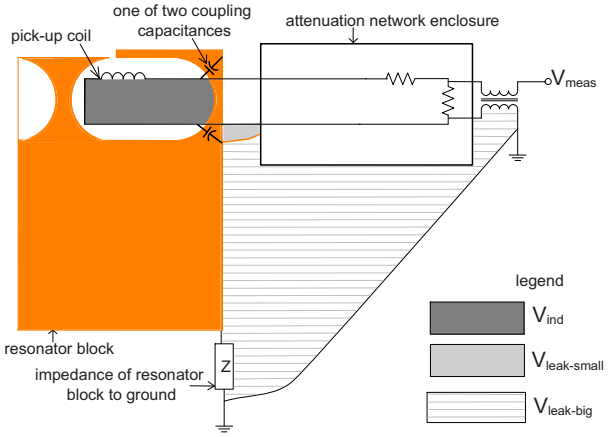

Fig. 4. Schematic showing a pick-up coil placed in a resonator cavity. The leakage voltage loops are also shown

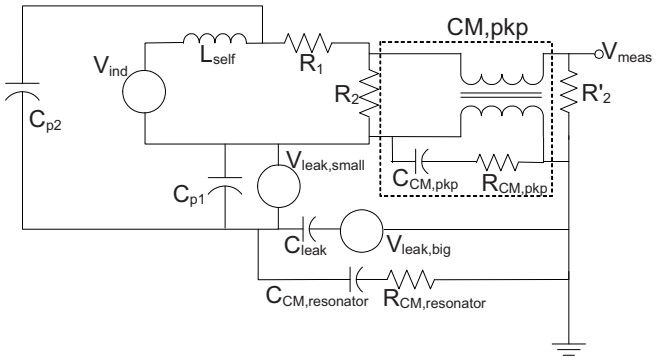

Fig. 5. Pick-up coil circuit showing the parasitic capacitive coupling and leakage voltage effects.

1) Expressions for induced and leakage voltages: The voltage induced in the reference pick-up coil when current I is circulating in the resonator cavities can be given as

$$V_{ind-ref-wo} \approx \mu_0 2\pi f \frac{I}{\ell} A_{pickup} \tag{7}$$

where μ_0 is the permeability of the free space, f is the frequency of operation, ℓ is the depth of the resonator cavities and A_{pickup} is the area of the pick-up coil in the resonator cavity. Voltages induced in the reference cavity when currents I_w, I_{wo} or I_{trim} flow in the resonator cavities can then be written using (7). When a thin-film sample of relative permeability μ^* is placed in the test cavity, the

voltage induced in the test pick-up coil is given by

$$V_{ind-test-w} \approx \mu_0 2\pi f \frac{I}{\ell}\Big[\mu^* A_{sample} + (A_{pickup} - A_{sample})\Big] \quad (8)$$

For calculating the voltages induced in the two ground loops shown due to the leakage flux, we have assumed that the flux from each of the resonator cavities is distributed uniformly in all the radial directions from the center of the cavity. $V_{leak-small}$ and $V_{leak-big}$ are then calculated as a fraction of V_{ind}. Fig. 4 shows schematically the two leakage flux loops.

$$V_{leak-small} = -0.08 \cdot V_{ind} \quad (9)$$

$$V_{leak-big} = -0.11 \cdot V_{ind} \quad (10)$$

C. Error Calculation

Based on the analysis in Section V-A and V-B the error in μ^* measurement can be calculated as described below.

When the parasitic capacitance, self inductance and leakage flux effects are neglected, the relative permeability of the sample can be written as

$$\mu^* = \frac{A_{pickup}}{A_{sample}} \left(\frac{V_{test-w}/V_{ref-w}}{V_{test-wo}/V_{ref-wo}} - 1 \right) + 1 \quad (11)$$

where V_{ref-w} (V_{test-w}) and V_{ref-wo} ($V_{test-wo}$) are the voltages measured at V_{meas} terminal of the reference (test) pick-up coil with and without the sample, respectively.

Let us assume that we have a thin-film sample with permeability $\mu^*_{assumed} = 50 - j1$. Using the values listed in Table I and as explained in Section V-A, we evaluate I_{wo}, I_w and I_{trim} for a given V_{source}. Subsequently, induced voltage in the test and reference pick-up coils can be obtained for different circulating currents as discussed in Section V-B1. Hence V_{ref-wo}, $V_{test-wo}$, V_{ref-w}, V_{test-w}, $V_{ref-trim}$ and $V_{test-trim}$ are obtained. In each of these, the first part of the subscript denotes whether it is the reference or the test pick-up coil and the part denotes the circulating current in the resonator cavities. Leakage voltages $V_{leak-small}$ and $V_{leak-big}$ are calculated for different induced voltages using (9) and (10).

When no sample is placed in the cavity, $V_{test-wo}$ and V_{ref-wo} are evaluated at resonance frequency, first neglecting $V_{leak-small}$, and then $V_{leak-big}$. Next, a sample is placed in the cavity and the system is allowed to go out of resonance and V_{test-w} and V_{ref-w} are calculated at a non-resonant frequency. These values of measured voltages are then used in (11) to obtain μ^*_{meas}. Hence we are able to examine the effect of each leakage voltage on the error in μ^* measurement. When a trimmer capacitor is used to maintain the LC circuit at resonance when the sample is in the cavity, C_{cav} changes to $C_{cav-trim}$ and hence $V_{test-trim}$ and $V_{ref-trim}$ are evaluated. The effects of the two leakage voltages on μ^* measurement are evaluated separately, similarly to when a trimmer capacitor is not used. Table IV lists μ^*_{meas} obtained under different conditions.

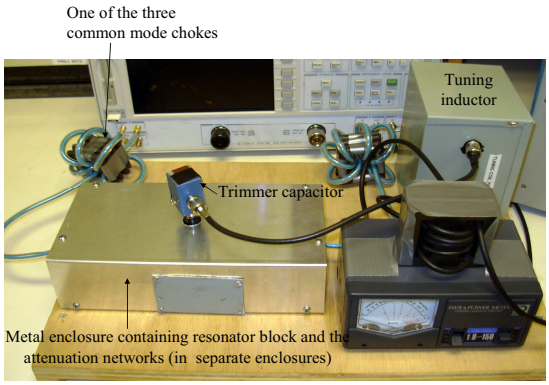

Fig. 6. Photograph of the complete system mounted on a board. The power amplifier is not shown.

From Table IV it can be seen that the maximum error in $\mu^{'}$ and $\mu^{''}$ measurement is about 1%. We are able to obtain μ^* measurements with and without using a trimmer capacitor. Based on this analysis we obtained experimental μ^* values with and and without a trimmer capacitor. These experimental results are discussed in Section VI.

TABLE IV
EFFECT OF LEAKAGE VOLTAGES ON μ^*_{meas} UNDER DIFFERENT CONDITIONS. $\mu^*_{assumed} = 50 - j1$

Condition	$V_{leak-big}$	$V_{leak-small}$
Without trimmer capacitor	50.01 - j0.99	49.99 - j0.993
With trimmer capacitor	50.01 - j1.01	49.99 - j1

D. Increasing the Ratio of Measured Voltages

One way to reduce the effect of noise and some other errors in μ^* measurements is to increase the percentage change in the signal when the sample is introduced into the coil. To do this, we decrease the air-flux signal when the sample is not present by changing the pick-up coil from a single loop to a figure-8 configuration. The two loops of the figure-8 encircle the air flux in opposite directions. As we need some signal for phase calibration, we have designed figure-8 pick-up coils for approximately 70% cancellation. The experimental results presented here were obtained with a figure-8 test pick-up coil.

E. Random Errors

Several steps are taken to keep the measuring system unchanged during the measurement process. The resonator cavity, pick-up coil attenuation networks and the 700 nH tuning coil are enclosed in aluminum boxes. The pick-up coil signals are run through semi-rigid coaxial cables and all the subsystems are mounted on a wooden board to keep them from moving. A window with a cover is machined on the resonator cavity enclosure for placing and removing the sample in the cavity. Fig. 6 is a photograph of the complete system.

VI. Experimental Results

As discussed in Section V, we should be able to obtain μ^* measurements both with and without using a trimmer capacitor. We obtained experimental measurements with the samples described in Section V. The experimentally observed resonant frequency, at which the measurements were taken, was 54.90 MHz. The reference calibrations for all data points were done individually and the experiment was repeated under identical nominal conditions. A pattern in $\mu^{''}$ variation with the increasing drive field was not directly visible. To analyze this data further we looked at the standard deviation among the 401 samples of phase measurement for each μ^* data point. The highest among these standard deviations was more than fifty times the lowest. We decided to use only those data points for which the standard deviation in phase measurement was up to ten times the lowest value. Figs. 8 and 9 represent the permeability measurements with this filtering scheme applied.

Approximately the first 100 phase samples out of the total 401 phase samples collected for each data point exhibited more random variations in phase than the rest and hence were regarded as being contaminated. This could be due to the fact that the power amplifier, which is switched off between measurements, takes some time to stabilize during which the phase data is contaminated. We ignored the initial contaminated samples for calculating the mean phase difference for each data point. One approach to reduce this error is to keep the power amplifier on at all times with its input turned to zero in between measurements.

The effectiveness of the pick-up coil to link all the flux through the thin-film sample when the sample is placed in the pick-up coil window (see Fig. 4) depends on the height of the pick-up coil. The pick-up coil links only a part of the flux as shown by two-dimensional finite element analysis in Fig. 7. This suggests that a correction factor should be applied to the μ^* measurements. For our test samples of length 4 mm, with a pick-up coil height of 3 mm, the ratio of the total flux in the sample to the flux linked by the pick-up coil as predicted two dimensional finite element analysis is 1.66. A three-dimensional simulation which takes into account the width of the sample is expected to give a more accurate value of the calibration factor that should be used. Presently we use a calibration factor obtained from a hard-axis BH-loop measurement for the sample with a Lakeshore 7300 series vibrating sample magnetometer. The relative permeability of the sample thus obtained is about 114.2 This suggests that the measured $\mu^{'}$ and $\mu^{''}$ values should be multiplied by a calibration factor, $K_{calibration} = 114.2/54.2$. Figs. 8 and 9 plot relative permeability calibrated in this manner. As can be seen from Figs. 8 and 9, $\mu^{'}$ remains constant with the increasing drive field while there is an upward trend in $\mu^{''}$ with increasing field. This suggests that the losses in Co-Zr-O thin-film material increase with flux density B at a rate higher than B^2.

Permeability measurements for the thin-film sample were made at low excitation fields using a Ryowa PMF-3000 permeance meter. The low-field permeability values in the 54 MHz region were found to be $\mu^{'}_{low-field} = 114.3$ and $\mu^{''}_{low-field} = 2.0 \pm 60\%$. The low-field $\mu^{''}$ value is higher than that obtained for high fields. However, the low-field $\mu^{''}$ measurement has a high degree of uncertainty associated with it. A large number of repeated measurements at high-fields are expected to help us establish a pattern in $\mu^{''}$ variation with drive field.

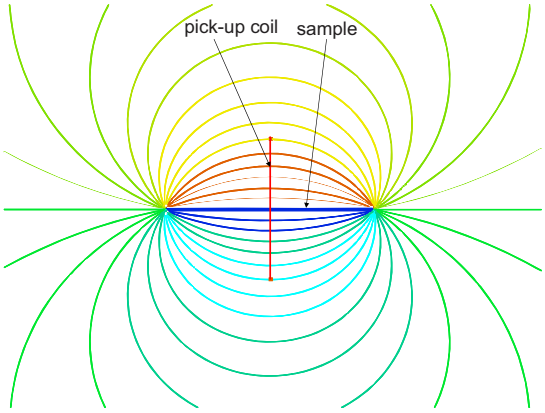

Fig. 7. Two-dimensional simulation result showing the percentage of flux in the sample that is linked by the pick-up coil.

VII. Conclusion

A high-field high-frequency permeance meter for thin-film materials used in high-power magnetic core inductors has been developed and tested. Errors, including those due to resonance frequency shift and the second-order coupling effects between the pick-up coil and resonator block are analyzed. Measurements are taken on Co-Zr-O samples based on this analysis and the results are compared against the low-field measurements. Increase in $\mu^{''}$ with the drive field is observed. A large number of repeated measurements at high-fields are expected to help us establish a pattern in $\mu^{''}$ variation with drive field.

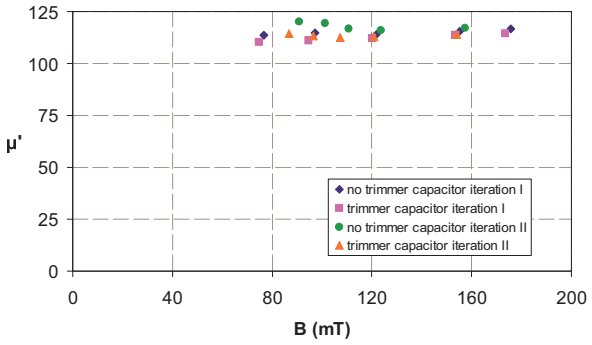

Fig. 8. Calibrated permeability measurements with a 12 μm thick Co-Zr-O sample.

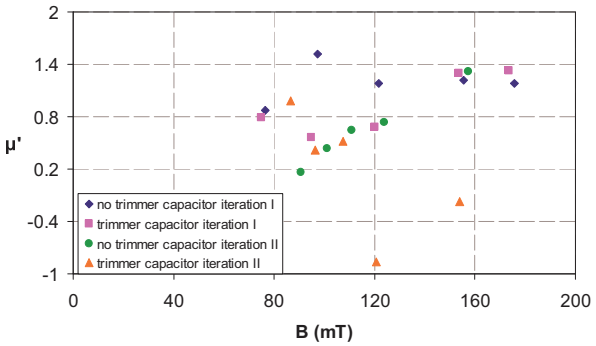

Fig. 9. Calibrated permeability measurements with a 12 μm thick Co-Zr-O sample.

REFERENCES

[1] J. Rivas, R. Wahby, J. Shafran, and D. Perreault, "New Architectures for Radio-Frequency dc/dc Power Conversion," in *35th IEEE Annual Power Electronics Specialists Conference.*, vol. 5, 2004, pp. 4074 – 4084.

[2] J. M. Rivas, D. Jackson, O. Leitermann, A. D. Sagneri, Y. Han, and D. J. Perreault, "Design considerations for very high frequency dc-dc converters," in *37th IEEE Power Electronics Specialists Conference*, 2006.

[3] J. M. Rivas, Y. Han, O. Leitermann, A. Sagneri, and D. Perreault, "A high-frequency resonant inverter topology with low voltage stress," in *38th IEEE Power Electronics Specialists Conference*, 2007.

[4] R. Pilawa-Podgurski, A. Sagneri, J. Rivas, D. Anderson, and D. Perreault, "Very high frequency resonant boost converters," in *38th IEEE Power Electronics Specialists Conference*, 2007.

[5] S. Prabhakaran, Y. Sun, P. Dhagat, W. Li, and C. Sullivan, "Microfabricated V-Groove Power Inductors for High-Current Low-Voltage Fast-Transient DC-DC Converters," *Power Electronics Specialists Conference, 2005. PESC '05. IEEE 36th*, pp. 1513–1519, 2005.

[6] S. Lu, Y. Sun, M. Goldbeck, D. Zimmanck, and C. Sullivan, "30-MHz Power Inductor Using Nano-Granular Magnetic Material," *Power Electronics Specialists Conference, 2007. PESC 2007. IEEE*, pp. 1773–1776, 17-21 June 2007.

[7] C. R. Sullivan, S. Prabhakaran, P. Dhagat, and Y. Sun, "Thin-film inductor designs and materials for high-current low-voltage power," in *Internationl Symposium on High-Frequency Micromagnetic Devices*, 2003.

[8] M. Yamaguchi, T. Kawazu, and K. Arai, "Resonance analysis of figure-8 coil type permeance meters," *IEEE Transactions on Magnetics*, vol. 29, no. 6, pp. 2986–2988, 1993.

[9] M. Yamaguchi, S. Yabukami, and K. Arai, "A new permeance meter based on both lumped elements/transmission line theories," *IEEE Transactions on Magnetics*, vol. 32, no. 5, pp. 4941–4943, 1996.

[10] ——, "A new 1 MHz-2 GHz permeance meter for metallic thin films," *IEEE Transactions on Magnetics*, vol. 33, no. 5, pp. 3619–3621, 1997.

[11] V. Korenivski, R. Van Dover, P. Mankiewich, Z.-X. Ma, A. Becker, P. Polakos, and V. Fratello, "A method to measure the complex permeability of thin films at ultra-high frequencies," *IEEE Transactions on Magnetics*, vol. 5, pp. 4905–4907, 1996.

[12] C. Grimes, P. Trouilloud, and R. Walser, "A new swept-frequency permeameter for measuring the complex permeability of thin magnetic films," *IEEE Transactions on Magnetics*, vol. 24, no. 1, pp. 603–610, Jan 1988.

[13] T. Kawazu, M. Yamaguchi, and K. Arai, "A new microstrip pickup coil for thin-film permeance meters," *IEEE Transactions on Magnetics*, vol. 30, no. 6, pp. 4641–4643, Nov 1994.

[14] C. Sullivan and S. Sanders, "Design of microfabricated transformers and inductors for high-frequency power conversion," *Power Electronics, IEEE Transactions on*, vol. 11, no. 2, pp. 228–238, Mar 1996.

[15] S. Ohnuma, H. J. Lee, N. Kobayashi, H. Fujimori, and T. Masumoto, "Co-Zr-O Nano-Granular Thin Films with Improved High Frequency Soft Magnetic Properties," *IEEE Transactions on Magnetics*, vol. 37, no. 4, pp. 3759–3761, Jul. 2001.

[16] "Soft ferrites and accessories," Datasheet - Ferroxcube Inc., 2001.

[17] Y. Shimada, M. Yamaguchi, S. Ohnuma, T. Itoh, W. D. Li, S. Ikeda, K. H. Kim, and H. Nagura, "Granular thin films with high RF permeability," *IEEE Transactions on Magnetics*, vol. 39, no. 5, pp. 3052–3056, Sept. 2003.

[18] P. Dhagat, S. Prabhakaran, and C. Sullivan, "Comparison of Magnetic Materials for V-Groove Inductors in Optimized High-Frequency DC-DC Converters," *IEEE Transactions on Magnetics*, vol. 40, no. 4, pp. 2008 – 2010, 2004.

[19] Y. Sun, W. Li, P. Dhagat, and C. Sullivan, "Perpendicular anisotropy in granular Co-Zr-O films," *Journal of Applied Physics*, vol. 97, no. 10, pp. 10N301–303, 2005.

[20] Y. Sun, C. Sullivan, W. Li, D. Kopp, F. Johnson, and S. Taylor, "Soft Magnetic Properties of Obliquely Deposited CoZrO Films," *IEEE Transactions on Magnetics*, vol. 43, no. 12, pp. 4060–4063, Dec. 2007.

[21] H. Klaus, "Design of permanent multipole magnets with oriented rare earth cobalt material," *Nuclear Instruments and Methods*, vol. 169, no. 1, 1980.